# Elastic Diffraction Scattering of Hadrons at High Energies*

G. Y. Chow and J. Rix
*Physics Department, Case Western Reserve University, Cleveland, Ohio 44106*
(Received 6 January 1969)

A new model for the high-energy ($p_{lab} \geq 4$ GeV/$c$) diffraction scattering of hadrons is presented. This shadow-scattering model explains, quantitatively, the magnitude and energy dependence of the widths of elastic-scattering diffraction peaks. An improved approximation for the inelastic intermediate states is used which emphasizes the role of quasielastic scattering and of optical absorption with energy-independent opacity. The quasielastic scattering is calculated from Feynman diagrams, while the optical absorption is constrained by the observed total cross section. Unitarity and one energy-independent scale-fixing parameter, then, give quantitative predictions for the widths of diffraction peaks which are only weakly dependent on the assumed $l$ dependence of the optical absorption.

## I. INTRODUCTION

THERE has been quite an extensive study of the elastic diffraction scattering of hadrons at high energies. The widths of the diffraction peaks are observed to depend on energy, but this energy dependence is not yet well understood. Single Regge-pole models give an indefinitely shrinking diffraction peak for all processes. When several Regge trajectories are introduced, the widths can shrink, grow, or stay relatively constant within a finite energy range, but a large number of parameters are involved. A recent analysis by Rarita *et al.*[1] used four Regge trajectories to fit all data of total cross sections, elastic differential cross sections, charge-exchange differential cross sections, ratio of real to imaginary part in the forward direction, and polarization. This fit required 31 parameters.

It has been suggested by Van Hove[2] that high-energy elastic scattering is the shadow of inelastic collisions. If it is assumed that the average number of particles produced in the inelastic collisions is large and the particles in the inelastic final states are uncorrelated (except for the constraint of energy-momentum conservation), Van Hove then shows that indefinite shrinkage is impossible. The Van Hove model gives a relation between the width of the diffraction peak and various average quantities associated with production experiments, e.g., multiplicities. The width also depends on the (unobservable) structure of the distribution function for transverse momenta of secondaries. This last fact prevents using the model for obtaining the energy dependence of the width in a simple manner. One observes, however, that growth, constancy or *limited* shrinkage are possible with this model.[3,4]

In this paper, we propose a unified model for all small-angle hadron diffraction scattering at high energies.[5] One would require that such a model explain both the magnitude and the energy dependence of all the widths of the diffraction peaks.

We begin with the assumption that the elastic scattering is the shadow of the inelastic collisions. Experiment[6] indicates that the inelastic cross section due to quasielastic scattering is not negligible at any energy. Quasielastic scattering is defined as those scattering events in which the incident particle undergoes an almost elastic diffraction scattering off the cloud of virtual particles surrounding the target particle. That is, the incident particle emerges with nearly all of its incident energy (in the laboratory system) and very few low-energy particles are produced from the virtual cloud. These collisions are evidently highly correlated and are not taken into account by the Van Hove model. This last fact is because an uncorrelated model favors having the production amplitudes strongly maximum when the produced particles all have nearly the same energy, namely, the average energy of a produced particle. Therefore, there would be no significant interference between quasielastic and uncorrelated amplitudes in the inelastic overlap integral. Our starting point will be to split the overlap function $g(s,t)$ into two parts; the quasielastic contribution $g_Q(s,t)$ and the rest $g_{V.H.}(s,t)$, which we will think of as arising primarily from uncorrelated production as suggested by Van Hove. The quasielastic part can be calculated by assuming it to be dominated by a certain class of Feynman diagrams as suggested by Drell and Hiida.[7] We will make as few assumptions as possible about $g_{V.H.}(s,t)$. The one of these assumptions which is most basic to the following work is that the average opacity[8] of $g_{V.H.}(s,t)$ is independent of energy (for $p_{lab} \geq 4$ GeV/$c$) *for all processes*, thus indicating a

* Work performed under the auspices of the U. S. Atomic Energy Commission. The work reported here is included in a thesis to be submitted by G. Y. Chow to the Case Western Reserve University in partial fulfillment of the requirement for the degree of Doctor of Philosophy.

[1] W. Rarita, R. J. Riddell, Jr., C. B. Chiu, and R. J. N. Phillips, Phys. Rev. **165**, 1615 (1968).

[2] L. Van Hove, Nuovo Cimento **28**, 798 (1963).

[3] W. N. Cottingham and R. F. Peierls, Phys. Rev. **137**, B147 (1965).

[4] J. J. J. Kokkedee, Nuovo Cimento **18**, 919 (1966).

[5] We concentrate on $pp$, $\bar{p}p$, $\pi^{\pm}p$, and $K^{\pm}p$ at $p_{lab} \geq 4$ GeV/$c$.

[6] E. W. Anderson, E. J. Bleser, G. B. Collins, T. Fujii, J. Menes, F. Turkot, R. A. Carrigan, Jr., R. M. Edelstein, N. C. Hien, T. J. McMahon, and I. Nadelhaft, Phys. Rev. Letters **16**, 855 (1966).

[7] S. D. Drell and K. Hiida, Phys. Rev. Letters **7**, 199 (1961).

[8] The average opacity will be defined later.

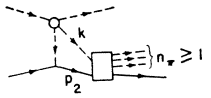


FIG. 1. Feynman diagram which is assumed to contribute to $\pi p$ quasielastic scattering. $n_\pi$ is the number of pions produced by a final state interaction, $k$ and $p_2$ are the four-momenta of the produced low-energy pion and the recoiled proton, and □ represents the final-state-interaction $S$ matrix.

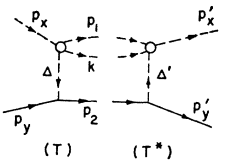


FIG. 2. The overlap function $g_Q(s,t)$ due to OPE diagram. The four-momentum of each line is labelled by the letter next to it.

certain universality. If we assume that the total cross section is known, the energy dependence of the total cross section and that of the quasielastic scattering will force $g_{V.H.}(s,t)$ to have a certain energy dependence. This, in turn, will determine the width of the elastic diffraction peaks.

In Sec. II, we begin by discussing the quasielastic scattering contribution to the overlap integral. Those readers not interested in the details of the quasielastic calculations should go directly to Sec. III, where we develop the formalism and approximations for calculating the widths. In Sec. IV, we present the numerical results and compare them with experiments. A few remarks and a prediction about $\pi\pi$ scattering are made in Sec. V.

## II. QUASIELASTIC SCATTERING

Let us first consider $\pi^+p$ quasielastic scattering. We assume that the main contribution is due to the Feynman diagram of Fig. 1, for which the incident particle can only lose a small amount of energy due to the phase-space restriction and the pion form factor. The intermediate pion $k$ and proton $p_2$ can be off the mass shell when there is a final-state interaction. We approximate this diagram by putting the virtual particles on the mass shell. However, it can be shown that the final-state interaction in the mass-shell approximation has no effect on $g_Q(s,t)$. That is, when the intermediate pion and nucleon of Fig. 1 are put on the mass shell and the diagram is put into the unitarity overlap integral, the resulting formula is exactly what one would have obtained by omitting all final-state interactions from Fig. 1. This is because the final-state interaction just multiplies the integrand of the overlap integral by a factor of $S^\dagger S=1$. The final-state interaction, therefore, can only change the correlation between the emerging low-energy pion and nucleon, and also change some of the three-particle final states into more-than-three-particle final states. Consequently, only the usual one-pion-exchange (OPE) diagram [Fig. 2($T$)] need be considered.

We should keep in mind, however, that we have calculated $g_Q(s,t)$ due to the whole diagram of Fig. 1. Therefore, even though only Fig. 2($T$) gives a nonvanishing contribution to $g_Q(s,t)$, one must not imagine that only three-particle final states contribute to quasielastic scattering.

The $T$ matrix is related to the $S$ matrix:

$$S=1+(2\pi)^4 i\delta^{(4)}(P_f-P_i)T, \tag{2.1}$$

where $P_i$ and $P_f$ are the total four-momenta of the initial and final states. The unitarity condition for the elastic scattering amplitude $T_{el}(s,t)$ is

$$\mathrm{Im}T_{el}(s,t)=\tfrac{1}{2}(2\pi)^4\sum_n \delta^{(4)}(P_n-p_x-p_y) \times T^\dagger(n;p_x',p_y')T(n;p_x,p_y), \tag{2.2}$$

where $p_x$ and $p_y$ are the four-momenta of the initial particles, $p_x'$ and $p_y'$ are the four-momenta of the final particles, $P_n$ is the total four-momentum of all the intermediate particles, $T(n;p_x,p_y)$ is the $T$ matrix for the transition from a two-particle state to an $n$-particle state, $s\equiv(p_x+p_y)^2$, and $t\equiv(p_x-p_x')^2$. The right-hand side may be decomposed into an elastic part, a quasielastic term, and the rest which arises primarily from uncorrelated production.

$$\begin{aligned}\mathrm{Im}T_{el}(s,t)=\tfrac{1}{2}(2\pi)^4\int \frac{d^3p_x''}{2W_{p_x''}}\frac{d^3p_y''}{E_{p_y''}/M}\delta^{(4)}(p_x''+p_y''-p_x-p_y)T_{el}^\dagger(p_x'',p_y'';p_x',p_y')T_{el}(p_x'',p_y'';p_x,p_y)\\ +\tfrac{1}{2}(2\pi)^4\sum_{Q.E.}\delta^{(4)}(p_1+k+p_2-p_x-p_y)T^\dagger(p_1,k,p_2;p_x',p_y')T(p_1,k,p_2;p_x,p_y)\\ +\tfrac{1}{2}(2\pi)^4\sum_{V.H.}\delta^{(4)}(P_n-p_x-p_y)T^\dagger(n;p_x',p_y')T(n;p_x,p_y)\equiv g_{el}(s,t)+g_Q(s,t)+g_{V.H.}(s,t),\end{aligned} \tag{2.3}$$

where $p_x''$ and $p_y''$ are the momenta of the elastic intermediate states, Q.E. and V.H. stand for quasielastic and uncorrelated states, respectively,

$$W_{p_x''}\equiv(\mathbf{p}_x''^2+\mu^2)^{1/2},\quad E_{p_y''}\equiv(\mathbf{p}_y''^2+M^2)^{1/2},$$

and $\mu$ and $M$ are the masses of a pion and a nucleon, respectively. The last line of Eq. (2.3) defines $g_{el}(s,t)$, $g_Q(s,t)$ and $g_{V.H.}(s,t)$, respectively, as the first, second, and third terms of the decomposition. In order to calculate $g_Q(s,t)$, we will need the $T$ matrix correspond-

ing to Fig. 2(T), which is given as follows with the spin indices written out explicitly:

$$T^{(s_r,s_i)}(p_1,k,p_2;\ p_x,p_y)=(2\pi)^3T(p_1,k;\ p_x,\ -\Delta)\times K(\Delta^2)(\Delta^2-\mu^2)^{-1}T^{(s_r,s_i)}(p_2;\ \Delta,p_y),\quad(2.4)$$

where $T^{(s_r,s_i)}(p_2;\ \Delta,p_y)$ is the matrix element for the three-particle vertex with point interaction, and $K(\Delta^2)$ is the pion form factor. The spins of the initial and intermediate protons are denoted by $s_i$ and $s_r$. We also assume that the off-mass-shell $\pi\pi$ amplitude $T(p_1,k;\ p_x,\ -\Delta)$ can be replaced by the mass-shell amplitude multiplied by a function of $\Delta^2$ only. Therefore,

$$T^{(s_r,s_i)}(p_1,k,p_2;\ p_x,p_y)=(2\pi)^3T(s_1,t')\phi(\Delta^2)\times(\Delta^2-\mu^2)^{-1}T(p_2;\ \Delta,p_y),\quad(2.5)$$

where $s_1\equiv(p_1+k)^2$, $t'\equiv(p_x-p_1)^2$, and $\phi(\Delta^2)$ is the product of the off-mass-shell correction and the pion form factor $K(\Delta^2)$. We will also need the elastic overlap function for $\pi\pi$ scattering,

$$g_{\mathrm{el}}{}^{\pi\pi}(s_1,t)=\tfrac{1}{2}(2\pi)^4\int\frac{d^3p_1}{2W_{p_1}}\frac{d^3k}{2W_k}\delta^{(4)}(p_1+k-p_x+\Delta)\times T^*(s_1,t'')T(s_1,t'),\quad(2.6)$$

where

$$t''\equiv(p_x'-p_1)^2,\quad W_{p_1}\equiv(\mathbf{p}_1{}^2+\mu^2)^{1/2},$$

and

$$W_k=(\mathbf{k}^2+\mu^2)^{1/2}.$$

The pion-nucleon vertex satisfies the following relation:

$$\sum_{s_r}(2\pi)^4\int\frac{d^3p_2}{E_{p_2}/M}T^{(s_r,s_f)\dagger}(p_2;\ \Delta',p_y')\times T^{(s_r,s_i)}(p_2;\ \Delta,p_y)\delta^{(4)}(p_y-p_2+\Delta)=[g^2/(2\pi)^5]\delta(s_2-M^2)\bar{u}(p_y',s_f)\times\tfrac{1}{2}\gamma\cdot(\Delta+\Delta')u(p_y,s_i),\quad(2.7)$$

where $s_2\equiv(p_y+\Delta)^2$, $E_{p_2}\equiv(\mathbf{p}_2{}^2+M^2)^{1/2}$, $\bar{u}(p_y',s_f)$, and $u(p_y,s_i)$ are the Dirac spinors of the final and initial protons, and the renormalized $\pi N$ coupling constant $g$ has the value $g^2/4\pi=14.4$. We then obtain the expression for the quasielastic overlap function,

$$\begin{aligned}g_Q(s,t)&=\tfrac{1}{2}\sum_{s_f,s_i,s_r}\tfrac{1}{2}(2\pi)^4\int\frac{d^3p_1}{2W_{p_1}}\frac{d^3k}{2W_k}\frac{d^3p_2}{E_{p_2}/M}\times\delta^{(4)}(p_1+k+p_2-p_x-p_y)\times T^{(s_r,s_f)\dagger}(p_1,k,p_2;\ p_x',p_y')\times T^{(s_r,s_i)}(p_1,k,p_2;\ p_x,p_y)\\&=\tfrac{1}{2}\sum_{s_f,s_i}\frac{g^2}{(2\pi)^3}\int ds_1d^4\Delta\delta(s_2-M^2)\times\delta[s_1-(p_x-\Delta)^2]\bar{u}(p_y',s_f)\tfrac{1}{2}\gamma\cdot(\Delta+\Delta')u(p_y,s_i)\times\frac{g_{\mathrm{el}}{}^{\pi\pi}(s_1,t)}{(\Delta^2-\mu^2)(\Delta'^2-\mu^2)}\phi(\Delta^2)\phi(\Delta'^2).\end{aligned}\quad(2.8)$$

Now assume that $s$ is large, and ignore the spin-flip term in $g_Q(s,t)$ [cf. Eq. (2.8)]. Then we can express $\bar{u}(p_y',s_f)\frac{1}{2}\gamma\cdot(\Delta+\Delta')u(p_y,s_i)$ in another form as done by Amati *et al.*[9] The spin-nonflip part of the overlap function is as follows:

$$g_Q(s,t)=\frac{g^2}{(2\pi)^3}\int ds_1g_{\mathrm{el}}{}^{\pi\pi}(s_1,t)d^4\Delta\times\frac{\delta(s_2-M^2)\delta[s_1-(p_x-\Delta)^2]}{(\Delta^2-\mu^2)(\Delta'^2-\mu^2)}\phi(\Delta^2)\phi(\Delta'^2)\times\left(-\frac{\Delta^2+\Delta'^2}{4M}+\frac{t}{4M}-\frac{ts_1}{4Ms}\right),\quad(2.9)$$

where

$$\Delta'^2=[(p_x-p_x')-\Delta]^2=t+\Delta^2-2(p_x-p_x')\cdot\Delta.\quad(2.10)$$

For large $s$, the last term in Eq. (2.10) is $s^{-1}$ smaller than the other terms; therefore, we will ignore it. Assume that the correction factor $\phi(\Delta^2)$ has the form suggested by Ferrari and Selleri,[10] namely,

$$\phi(\Delta^2)=\alpha/(\alpha-\Delta^2+\mu^2);\quad(2.11)$$

then we obtain the formula

$$g_Q(s,t)=\frac{g^2}{(2\pi)^3}\int ds_1g_{\mathrm{el}}{}^{\pi\pi}(s_1,t)d^4\Delta\times\frac{\delta[s_2-M^2]\delta[s_1-(p_x-\Delta)^2]}{(\Delta^2-\mu^2)(\Delta^2+t-\mu^2)}\times\frac{\alpha}{\alpha-\Delta^2+\mu^2}\frac{\alpha}{\alpha-\Delta^2-t+\mu^2}\left(-\frac{\Delta^2}{2M}-\frac{ts_1}{4Ms}\right).\quad(2.12)$$

Define the following separation:

$$g_Q(s,t)\equiv g_Q{}^{(1)}(s,t)+g_Q{}^{(2)}(s,t),\quad(2.13)$$

TABLE I. Quantum numbers of quarks.

| | Baryon No. | Charge | Strangeness | Isospin |
|---|---|---|---|---|
| $\mathcal{P}$ | $\frac{1}{3}$ | $\frac{2}{3}e$ | 0 | $\frac{1}{2}$ |
| $\mathfrak{N}$ | $\frac{1}{3}$ | $-\frac{1}{3}e$ | 0 | $\frac{1}{2}$ |
| $\lambda$ | $\frac{1}{3}$ | $-\frac{1}{3}e$ | $-1$ | 0 |

[9] D. Amati, A. Stangehllini, and S. Fubini, Nuovo Cimento 26, 896 (1962).
[10] E. Ferrari and F. Selleri, Phys. Rev. Letters 7, 387 (1961).

where $g_Q^{(1)}(s,t)$ and $g_Q^{(2)}(s,t)$ are the first and second terms on the right-hand side of Eq. (2.12), respectively. The $d^4\Delta$ integration of $g_Q^{(1)}(s,t)$ can be carried out with the following result:

$$g_Q^{(1)}(s,t)=\frac{g^2}{(2\pi)^3}\int_{4\mu^2}^{(s^{1/2}-M)^2} ds_1 g_{el}^{\pi\pi}(s_1,t)\left[\frac{\pi}{2Ms}\frac{\alpha}{-t}\left(-\frac{\mu^2+\alpha}{\alpha+t}\ln\frac{\alpha+\mu^2+\psi_1+\psi_2}{\alpha+\mu^2+\psi_1-\psi_2}+\frac{\mu^2+\alpha-t}{\alpha-t}\ln\frac{\alpha-t+\mu^2+\psi_1+\psi_2}{\alpha-t+\mu^2+\psi_1-\psi_2}\right.\right.$$
$$\left.\left.-\frac{\mu^2}{\alpha-t}\ln\frac{\mu^2+\psi_1+\psi_2}{\mu^2+\psi_1-\psi_2}+\frac{\mu^2-t}{\alpha+t}\ln\frac{\mu^2-t+\psi_1+\psi_2}{\mu^2-t+\psi_1-\psi_2}\right)\right], \quad (2.14)$$

where $\psi_1=\frac{1}{2}(s-s_1+M^2)$ and $\psi_2=\frac{1}{2}[s^2+M^4+s_1^2-2ss_1-2M^2s_1-2M^2s]^{1/2}$. It can be shown that the $t$ dependence of the factor in square brackets of Eq. (2.14) is very weak compared to that in $g_{el}^{\pi\pi}(s_1,t)$. Therefore, we can ignore that $t$ dependence of this factor and evaluate it at $t=0$. Furthermore, $g_Q^{(2)}(s,t)$ is very small compared to $g_Q^{(1)}(s,t)$ for small $t$ ($\simeq 5\%$).

The elastic overlap function for $\pi\pi$ scattering presumably has nearly the same shape as that for $\pi N$ or $K\pi$ scattering, the sizes being different. In addition, we anticipate that the shape of the elastic $\pi\pi$ overlap function should have rather weak energy dependence, and similarly for $\pi N$ or $K\pi$. These conjectures suggest that the quasielastic $\pi N$ overlap function should have the following form:

$$g_Q^{\pi N}(s,t)\equiv\Gamma^{\pi N}(s,t)g_{el}^{\pi\pi}(s,t), \quad (2.15)$$

where $\Gamma^{\pi N}(s,t)$ is a smooth function of $t$ slowly varying compared to $g_{el}^{\pi\pi}(s,t)$. The function $\Gamma^{\pi N}(s,t)$ can then be approximated by its value at $t=0$,

$$g_Q^{\pi N}(s,t)\simeq\Gamma^{\pi N}(s,0)g_{el}^{\pi\pi}(s,t). \quad (2.16)$$

provided the following condition is satisfied:

$$\frac{d}{dt}\ln\frac{g_{el}^{\pi\pi}(s_1,t)}{g_{el}^{\pi\pi}(s,t)}\bigg|_{t=0}\ll\frac{d}{dt}\ln[g_{el}^{\pi\pi}(s,t)]\bigg|_{t=0}. \quad (2.17)$$

This condition [Eq. (2.17)], which requires that the width of the elastic diffraction peak to be a weak function of energy will specify a range of $s$ and $s_1$ for which $\Gamma^{\pi N}(s,0)$ as calculated by the following equation can be used in Eq. (2.16) with small error:

$$\Gamma^{\pi N}(s,0)\equiv\int_{4\mu^2}^{(s^{1/2}-M)^2} ds_1 K^{\pi N}(s,s_1)\frac{g_{el}^{\pi\pi}(s_1,0)}{g_{el}^{\pi\pi}(s,0)}. \quad (2.18)$$

The integrand $K^{\pi N}(s,s_1)$ will be implicitly defined later. There is another approximation which we will use in Sec. III. That is, to define a new final relation

$$g_Q^{\pi N}(s,t)\simeq R^{\pi N}(s)g_{el}^{\pi N}(s,t), \quad (2.19)$$

where

$$R^{\pi N}(s)\equiv\Gamma^{\pi N}(s,0)\, g_{el}^{\pi\pi}(s,0)/g_{el}^{\pi N}(s,0). \quad (2.20)$$

Equation (2.19) should be a good approximation if the following holds:

$$\frac{d}{dt}\ln\frac{g_{el}^{\pi\pi}(s,t)}{g_{el}^{\pi N}(s,t)}\bigg|_{t=0}\ll\frac{d}{dt}\ln[g_{el}^{\pi N}(s,t)]\bigg|_{t=0}, \quad (2.21)$$

meaning that the various elastic widths are to be of similar size. In an exactly similar manner, $g_Q^{NN}(s,t)$ and $g_Q^{KN}(s,t)$ can be derived and put in approximate forms analogous to Eq. (2.16) or Eq. (2.19). One remark should be made here. It is clear by now that our intention for this paper is to calculate the sizes and the energy dependence of all the elastic diffraction widths. As we will notice later, the width is directly related to the shape of the overlap function [cf. Eq. (3.14)]. Therefore, at first sight it seems that in approximations (2.16) and (2.19) we have already fixed the sizes and the energy dependence of all the diffraction widths. However, one should notice that our approach is essentially perturbative, i.e., if the difference in sizes of all the widths and the energy dependence of the widths are first-order effects, we can calculate them by using, as input, the widths with these first-order effects ignored. Then, in Sec. V, we will indicate that such an approach is sensible. In the $NN$ case, the spin of the upper "high"-energy vertex, corresponding to Fig. 2, is ignored. The introduction of isotopic spin presents no difficulties.

The resulting expression for $R(s)$ and $\Gamma(s,0)$ [via Eq. (2.20)] is given by the following integral:

$$R^{xp}(s)=\frac{g^2M^2}{2\pi^2}\int_{(\mu+M_x)^2}^{(s^{1/2}-M)^2}\frac{2q_1^{x}s_1^{1/2}}{s}ds_1 D^{xp}(s_1)\frac{f(s,s_1)}{g(s,s_1,M_x^2)}$$
$$\times C(s,s_1,M_x^2), \quad (2.22)$$

where

$$C(s,s_1,M_x^2)$$
$$=\frac{1}{2M^2}\left(\frac{(B_1-B_2)(B_1+B_2)}{2B_2}\left(1+\frac{2\mu^2}{\alpha}\right)\right.$$
$$\times\ln\frac{(B_1+B_2)(\alpha+B_1-B_2)}{(B_1-B_2)(\alpha+B_1+B_2)}-\mu^2$$
$$\left.-\frac{(B_1-B_2)(B_1+B_2)}{(\alpha+B_1+B_2)(\alpha+B_1-B_2)}(\mu^2+\alpha)\right), \quad (2.23)$$

$$B_1=(s+M^2-s_1)(s+M^2-M_x^2)/2s$$
$$+\mu^2-2M^2, \quad (2.24)$$

$$B_2=(1/2s)\{[(s+M^2-s_1)^2-4M^2s]$$
$$\times[(s-M^2-M_x^2)^2-4M^2M_x^2]\}^{1/2}, \quad (2.25)$$

$$f(s,s_1)=[s-(s_1^{1/2}+M)^2]^{1/2}[s-(s_1^{1/2}-M)^2]^{1/2}, \quad (2.26)$$

$$g(s,s_1,M_x^2)$$
$$=4[(2M^2-\mu^2)^2 s+M^2(s-s_1+M^2)^2$$
$$+M^2(s-M^2-M_x^2)^2-4M^4M_x^2$$
$$-(2M^2-\mu^2)(s-s_1+M^2)(s+M^2-M_x^2)], \quad (2.27)$$

$$q_1^{xp}=(2s_1^{1/2})^{-1}[s_1^2+M_x^4+\mu^4-2\mu^2 s_1$$
$$-2M_x^2 s_1-2\mu^2 M_x^2]^{1/2}, \quad (2.28)$$

$$D^{xp}(s_1)=[2\sigma_{el}^{x\pi^+}(s_1)+\sigma_{el}^{x\pi^0}(s_1)]/\sigma_{el}^{xp}(s). \quad (2.29)$$

The superscript $x$ denotes the particular process of interest, and the corresponding mass is $M_x$; e.g., for $\pi^+p$ scattering, $x$ is $\pi^+$, and $M_x$ is $\mu$. Eqs. (2.22)–(2.29) are the final formulas for $R(s)$, the ratio of quasielastic cross section to the elastic cross section. A number of assumptions have gone into these formulas. Before going further, it is worthwhile to recapitulate all of these assumptions and approximations so that one can see the basis on which the results rest. For all of the processes of interest ($pp$, $\bar{p}p$, $\pi^{\pm}p$, and $K^{\pm}p$), we have assumed that the following assumptions are valid when the total energy squared $s$ of the initial particles is large compared to the square of the nucleon mass, and the four-momentum transfer $t$ is small [$|t|\lesssim 0.5$ (GeV/$c$)$^2$]: (a) The quasielastic scattering is mainly due to the OPE diagram [cf. Fig. 2(T) and Eq. (2.4)]. (b) The off-mass-shell amplitude at the upper vertex of Fig. 2(T) can be replaced by the corresponding on-mass-shell amplitude multiplied by a universal function $\phi(\Delta^2)$, given by Eq. (2.11). (c) The spin-flip part in the quasielastic overlap function $g_Q(s,t)$ is ignored [cf. Eq. (2.8)]. (d) The last term in Eq. (2.10) is ignored. (e) The $t$ dependence of the factor in square brackets in Eq. (2.14) is ignored. (f) $g_Q^{(2)}(s,t)$, as defined by Eqs. (2.12) and (2.13), is ignored. (g) The elastic overlap functions for $\pi\pi$ and $K\pi$ scattering are assumed to have the same functional form with respect to $t$ as that for $\pi p$ scattering, although the parameters that enter into the function can be different for the different processes. (h) The shapes of the elastic overlap functions of $\pi\pi$, $K\pi$, $\pi p$, and $NN$ have weak energy dependence [cf. Eq. (2.16)]. (i) The elastic diffraction widths for different processes have approximately the same size [cf. Eq. (2.19)]. This assumption can be relaxed without affecting the results appreciably, as will be discussed in Sec. V. (j) For the quasielastic scattering of $NN$, the spin at the upper vertex of Fig. 2(T) is ignored.

It is an unfortunate fact that we do not have data on the cross sections for meson-meson scattering. We will use estimates of these given by the quark model in Lipkin's version.[11] This version gives a good agreement between meson-baryon total cross sections. The assumptions are the following: (a) The basic additivity assumption that the scattering amplitude is just the sum of quark-quark scattering amplitudes. (b) The quark-quark amplitudes satisfy the following relations:

$$(\mathcal{P}\mathfrak{N})=(\bar{\mathcal{P}}\mathfrak{N})=(\mathcal{P}\mathcal{P})=(\mathfrak{N}\mathfrak{N})\equiv\bar{P}, \quad (2.30)$$

$$(\lambda\mathcal{P})=(\lambda\mathfrak{N})=(\bar{\lambda}\mathcal{P})=(\bar{\lambda}\mathfrak{N})\equiv\bar{P}-\bar{S}, \quad (2.31)$$

and

$$(\bar{\mathcal{P}}\mathcal{P})=(\bar{\mathfrak{N}}\mathfrak{N})\equiv\bar{P}+\bar{A}. \quad (2.32)$$

The symbol $(\mathcal{P}\mathfrak{N})$ denotes the amplitude for $\mathcal{P}$- and $\mathfrak{N}$-quark scattering. The three quarks $\mathcal{P}$, $\mathfrak{N}$, and $\lambda$ have the quantum numbers given in Table I. The common amplitude for the nonstrange quarks and antiquarks is denoted by $\bar{P}$, while the symbol $\bar{S}$ represents the contribution of $SU(3)$ symmetry breaking in the strange-quark scattering, and finally $\bar{A}$ corresponds to the annihilation contribution.

With this model, all of the total cross sections of hadron scattering can be expressed in terms of three total cross sections. However, the predictions of baryon-baryon total cross sections by using meson-baryon data are too small by about 15%. This fact is likely because the effective quark-quark scattering in baryons and in mesons is not the same. In order to remedy this discrepancy, we introduce a factor $\gamma$, which is chosen as follows:

$$\gamma\equiv\sigma_T^{NN}(\infty)_{\text{ext.}}/\sigma_T^{NN}(\infty)_{\text{Q.M.}}, \quad (2.33)$$

where "ext." implies extrapolated from experiment, while Q.M. implies predicted by the quark model. For meson-baryon cross sections, we use the quark-model predictions unaltered. For baryon-baryon cross sections, we multiply the cross sections predicted by the quark model by the factor $\gamma$ and for meson-meson cross sections by $\gamma^{-1}$. Now the predicted total baryon-baryon cross section (with correction) agrees well with experiments. The meson-meson total cross sections can be expressed in the following way:

$$\sigma_T^{K^+\pi^0}=(4\bar{P}+\tfrac{1}{2}\bar{A}-2\bar{S})/\gamma, \quad (2.34)$$

$$\sigma_T^{K^+\pi^+}=(4\bar{P}-2\bar{S})/\gamma, \quad (2.35)$$

$$\sigma_T^{K^-\pi^0}=\sigma_T^{K^+\pi^0}, \quad (2.36)$$

$$\sigma_T^{K^-\pi^+}=(4\bar{P}+\bar{A}-2\bar{S})/\gamma, \quad (2.37)$$

$$\sigma_T^{\pi^+\pi^0}=(4\bar{P}+\bar{A})/\gamma, \quad (2.38)$$

$$\sigma_T^{\pi^+\pi^+}=4\bar{P}/\gamma, \quad (2.39)$$

$$\sigma_T^{\pi^-\pi^+}=(4\bar{P}+2\bar{A})/\gamma, \quad (2.40)$$

$$\sigma_T^{\pi^-\pi^0}=\sigma_T^{\pi^0\pi^0}=\sigma_T^{\pi^+\pi^0}. \quad (2.41)$$

We will choose the total cross sections of $\pi^{\pm}p$ and $K^+p$ to determine $\bar{P}$, $\bar{A}$, and $\bar{S}$,

$$\bar{P}=\tfrac{1}{6}(2\sigma_T^{\pi^+p}-\sigma_T^{\pi^-p}), \quad (2.42)$$

$$\bar{A}=(\sigma_T^{\pi^-p}-\sigma_T^{\pi^+p}), \quad (2.43)$$

$$\bar{S}=\tfrac{1}{3}(2\sigma_T^{\pi^+p}-\sigma_T^{\pi^-p}-\sigma_T^{K^+p}). \quad (2.44)$$

[11] H. J. Lipkin, Phys. Rev. Letters **16**, 1015 (1966).

One remark should be made here. When we use meson-baryon cross sections to predict meson-meson or baryon-baryon cross sections, they should be evaluated in such a way that the quark-quark scattering has the same amount of energy. For baryon-baryon scattering, each quark-quark pair has energy $\frac{1}{3}\sqrt{s}$, for meson-baryon each pair has $(5/12)\sqrt{s}$, while for meson-meson each pair has $\frac{1}{2}\sqrt{s}$. Therefore, meson-baryon cross sections at total energy $\sqrt{s_{\pi N}}$ can be used to predict baryon-baryon cross sections at $(5/4)\sqrt{s_{\pi N}}$ and meson-meson cross sections at $\frac{5}{6}\sqrt{s_{\pi N}}$.

Now it is possible, using these quark results, to obtain expressions for $D^{xp}(s_1)$ that involve only observable processes. The range of $s_1$ in the integration of Eq. (2.22) extends from threshold nearly to $s$. However, the integrand is a function which peaks about a value of $s_1$ which depends on $s$. For example, when $s=20$ GeV$^2$ for $p$-$p$ scattering, the integrand is sharply peaked about $s_1=6.2$ GeV$^2$, while at higher energy, $s=52$ GeV$^2$, the integrand is broadly peaked about $s_1=15.8$ GeV$^2$. These facts indicate that even when $s$ is at high energy, the diffraction scattering prefers to take place at an intermediate energy. One will obtain an unreliable value for $R^{xp}(s)$ by making a high-energy approximation for $D^{xp}(s_1)$ unless $s$ is very large ($p_{\rm lab}\gtrsim 15$ GeV/$c$). In practice, one takes experimental values for $\sigma_{\rm el}(s_1)$ if $s_1\lesssim 4.53$ GeV$^2$ and uses $\sigma_{\rm el}(s_1)\propto\sigma_T^2(s_1)$ if $s_1\gtrsim 4.53$ GeV$^2$. This approximation will be discussed in detail in Sec. IV.

We would add that our model for quasielastic scattering implicitly contains absorption corrections. That is because the correction factor [Eq. (2.11)] is adjusted to agree with experiments. Since the average opacity is taken to be energy-independent, the absorption correction will also be energy-independent, and the correction is then just a scale factor, which can be incorporated into Eq. (2.11) by a suitable choice of $\alpha$.

## III. GENERAL FORMALISM AND APPROXIMATIONS

We define the elastic amplitude $T_{\rm el}(s,t)$ in terms of the spin-nonflip amplitude $g_1(s,t)$ and the spin-flip amplitude $g_2(s,t)$ as

$$T_{\rm el}(s,t)=g_1(s,t)+i\boldsymbol{\sigma}\cdot\mathbf{n}\sin\theta\, g_2(s,t), \tag{3.1}$$

where the scattering angle is given by $\theta$. Predazzi[12] has observed from the recent $\pi^{\pm}p$ polarization data[13] that $g_1(s,0)$ and $g_2(s,0)$ are of the same order of magnitude. Since the elastic differential cross section is proportional to $|g_1(s,t)|^2+\sin^2\theta\,|g_2(s,t)|^2$, the spin-flip contribution is smaller by a factor of $\sin^2\theta\simeq -t/s$, which is negligible for the energies and momentum transfers in which we are interested. Therefore, we ignore all but the spin-nonflip amplitudes in what follows. Furthermore, we also ignore the real part of the amplitude at energies $p_{\rm lab}\gtrsim 4$ (GeV/$c$), because it is observed experimentally to be small. The real part of the amplitude always enters in our equations squared. In the special case that the real part has the same $t$ dependence as the imaginary part, the real part can be incorporated easily into the equation for the slope, giving a small improvement to the results.

The elastic-scattering amplitude $T_{\rm el}(s,t)$ and the overlap functions $g_{\rm V.H.}(s,t)$ and $g_{\rm Q}(s,t)$, can be expanded in terms of the partial-wave amplitudes $h_l(s)$, $\rho_l^{\rm V.H.}(s)$, and $\rho_l^{\rm Q}(s)$, respectively,

$$T_{\rm el}(s,t)=\frac{\sqrt{s}}{8\pi^5 q}\sum_l (2l+1)h_l(s)P_l(\cos\theta), \tag{3.2}$$

$$g_{\rm V.H.}(s,t)=\frac{\sqrt{s}}{16\pi^5 q}\sum_l (2l+1)\rho_l^{\rm V.H.}(s)P_l(\cos\theta), \tag{3.3}$$

$$g_{\rm Q}(s,t)=\frac{\sqrt{s}}{16\pi^5 q}\sum_l (2l+1)\rho_l^{\rm Q}(s,t)P_l(\cos\theta), \tag{3.4}$$

where the momentum in the c.m. system is $q$, and $\cos\theta\simeq 1-2t/s$ at $p_{\rm lab}\gtrsim 4$ GeV/$c$. According to Eq. (2.19), $\rho_l^{\rm Q}(s)$ takes the following form:

$$\rho_l^{\rm Q}(s)\simeq 4R(s)\,|h_l(s)|^2. \tag{3.5}$$

The unitarity condition is given as

$$\mathrm{Im}h_l(s)=[1+R(s)]\,|h_l(s)|^2+\tfrac{1}{4}\rho_l^{\rm V.H.}(s). \tag{3.6}$$

The cross sections and the slope of the diffraction peak $b(s)$ (i.e., width inverse) can be expressed as

$$\sigma_T(s)=\frac{4\pi}{q^2}\sum_l (2l+1)\,\mathrm{Im}h_l(s), \tag{3.7}$$

$$\sigma_{\rm inel}(s)=\frac{\pi}{q^2}\sum_l (2l+1)[\rho_l^{\rm V.H.}(s)+\rho_l^{\rm Q}(s)], \tag{3.8}$$

$$\frac{d\sigma_{\rm el}}{dt}(s)=\pi\left|\sum_l (2l+1)\frac{h_l(s)}{q^2}P_l(\cos\theta)\right|^2, \tag{3.9}$$

$$b(s)\equiv\frac{d}{dt}\ln\frac{d\sigma_{\rm el}}{dt}\bigg|_{t=0}\simeq\frac{8\pi}{\sigma_T(s)sq^2}\times\sum_l (2l+1)l(l+1)\,\mathrm{Im}h_l, \tag{3.10}$$

where the real part has been neglected in Eq. (3.10). Since we have assumed $h_l(s)$ to be pure imaginary, the unitarity condition is satisfied by

$$\mathrm{Im}h_l(s)=\frac{1-\{1-\rho_l^{\rm V.H.}(s)[1+R(s)]\}^{1/2}}{2[1+R(s)]}. \tag{3.11}$$

Let us assume that $\rho_l^{\rm V.H.}(s)$ represents grey-sphere absorption. This is the simplest $l$ dependence to deal

[12] E. Predazzi and G. Soliani, Nuovo Cimento **51**, 427 (1967).
[13] M. Borghini, G. Coignet, L. Dick, K. Kuroda, L. DiLella, P. C. Macq, A. Michalowicz, and J. C. Olivier, Phys. Letters **21**, 114 (1966); **24B**, 77 (1967).

with. In Sec. V, we show that the resulting predictions for $b(s)$ are insensitive to the choice of $l$ dependence for $\rho_l^{\text{V.H.}}$ provided that $\rho_l^{\text{V.H.}}$ is subject to several constraints, to be discussed below. In addition to the important assumption of shadow scattering [Eq. (3.11)], we will assume that *the average opacity of* $\rho_l^{\text{V.H.}}$ *is a constant function of s for all processes* for $p_{\text{lab}} \gtrsim 4$ GeV/$c$. This represents the first constraint on $\rho_l^{\text{V.H.}}$ and is a very important aspect of our model. The average opacity $\epsilon$ is defined as follows:

$$\epsilon(s) \equiv [\sum_l (2l+1)\rho_l^{\text{V.H.}}(s)]^2 / [2\sum_l (2l+1)l(l+1)\rho_l^{\text{V.H.}}(s)] \simeq \text{const for } p_{\text{lab}} \gtrsim 4 \text{ GeV}/c. \quad (3.12)$$

Furthermore, we assume that the $\rho_l^{\text{V.H.}}$'s have the same shape for all processes except that the parameters may be different. For the case presently of interset, $\rho_l^{\text{V.H.}}$ has the form

$$\rho_l^{\text{V.H.}}(s) = \epsilon \sum_{j=0}^{L} \delta_{j,l}, \quad (3.13)$$

where $L$=nearest integer to $qR_{\text{V.H.}}(s)$. The range $R_{\text{V.H.}}$ of the uncorrelated absorption is a function of energy to be determined. For the grey sphere, the average opacity [Eq. (3.12)] is just $\epsilon$ of Eq. (3.13) which we take as an energy-independent parameter also to be determined. When one combines the previous relations into Eq. (3.10), the final relation for $b(s)$ results:

$$b(s) \simeq \tfrac{1}{4} R_{\text{V.H.}}^2(s) \simeq \frac{\sigma_T(s)[1+R(s)]}{8\pi[1-\{1-\epsilon[1+R(s)]\}^{1/2}]}. \quad (3.14)$$

This formula will be used in Sec. IV to calculate the slope $b(s)$. The right-hand side contains only known quantities: $\sigma_T(s)$ comes directly from experimental data, $R(s)$ is calculated according to Eqs. (2.22)–(2.29), and $\epsilon$ is to be determined by Eqs. (3.15)–(3.23). Let us again recapitulate all of the assumptions and approximations which have gone into Eq. (3.14). (a) The spin-flip part in the elastic-scattering amplitude is ignored [cf. Eq. (3.1)]. (b) The real part of the elastic-scattering amplitude is ignored. (c) The partial-wave expansion of the overlap function $\rho_l^{\text{V.H.}}(s)$ has a grey-sphere shape. Other shapes are discussed in Sec. V. (d) The average opacity of $\rho_l^{\text{V.H.}}(s)$ is energy-independent. It is one of the most important assumptions in our model.

These four assumptions are expected to be valid when $p_{\text{lab}} \gtrsim 4$ (GeV/$c$) and $|t| \lesssim 0.5$ (GeV/$c$)$^2$. All of the assumptions that are necessary for obtaining the formulas of Secs. II and III have been summarized in the paragraphs after Eqs. (2.29) and (3.14) except those concerning the applicability of the quark model to meson-meson scattering which appear in Eqs. (2.30)–(2.33) and those concerning the calculation of $\epsilon$, which appear in Eqs. (3.19)–(3.23). In the absence of the quasielastic contribution ($R$=0), the energy dependence of $b(s)$ is governed by $\sigma_T(s)$. Since all $\sigma_T(s)$ appear to decrease to constant values, one would obtain *decreasing* $b$ (growth of the diffraction peak) for all processes. The factor $R(s)$ also decreases to a constant value with energy, and if $\sigma_T$ were constant (e.g., $pp$ and $K^+p$ scattering for $p_{\text{lab}} \gtrsim 6$ GeV/$c$), $b$(s) for that process would *increase* for any value of $\epsilon$ (shrinkage of the diffraction peak).

Evidently, the observed behavior of the diffraction peaks at high energies depends on a balance between these opposing effects. Let us now discuss the average opacity parameter $\epsilon$.

It is known that the size of the interaction region of a nucleon is roughly the same as that of a meson. Therefore, we expect that

$$R_{\text{V.H.}}^{NN} \simeq R_{\text{V.H.}}^{\pi N} \simeq R_{\text{V.H.}}^{KN} \simeq R_{\text{V.H.}}^{\pi\pi} \simeq R_{\text{V.H.}}^{K\pi} \quad (3.15)$$

or

$$b^{NN} \simeq b^{\pi N} \simeq b^{KN} \simeq b^{\pi\pi} \simeq b^{K\pi}. \quad (3.16)$$

We will assume that at *infinite energy* all the $b$'s would be the same if the quark model were exact, that is, if $\gamma$=1, or, alternatively,

$$\sigma_T^{NN}(\infty)/\sigma_T^{\pi N}(\infty) = \sigma_T^{\pi N}(\infty)/\sigma_T^{\pi\pi}(\infty) = \tfrac{3}{2}, \quad (3.17)$$

and

$$\sigma_T^{\pi N}(\infty) = \sigma_T^{KN}(\infty). \quad (3.18)$$

However, the quark model is not exact, i.e., $\gamma \neq 1$. Consequently, $\sigma_T^{NN}(\infty)$ is modified by $\gamma$ and $\sigma_T^{\pi\pi}(\infty)$ by $\gamma^{-1}$. We assume that the breakage affects the $b$'s but does not affect the $\epsilon$'s. This point of view results because we associate the ranges $R_{\text{V.H.}}$ (and consequently $b$) with masses whose degeneracy are significantly affected by the breakage induced by changes in binding energy, while the $\epsilon$'s are presumed to be dependent on coupling constants which are less affected by breakage. We can calculate the $\epsilon$'s and $b$'s at infinite energy by using this last reasoning. Notice that the calculated quasielastic factors $R^{NN}(\infty)$, $R^{\pi N}(\infty)$, and $R^{KN}(\infty)$ are equal. The $\epsilon$'s must satisfy the relation

$$b^U = \frac{\sigma^{xy}(\infty)[1+\gamma^2 R^{xy}(\infty)]}{8\pi\{1-[1-\epsilon_{xy}(1+\gamma^2 R^{xy}(\infty))]^{1/2}\}}, \quad (3.19)$$

where $R^{xy}(\infty) = R(\infty)$, $\sigma^{xy}$ is given by *exact* quark relations [Eqs. (3.17 )and (3.18)] in terms of $\sigma_T^{\pi N}(\infty)$ extrapolated from experiment which fixes the scale, and $b^U$ is the universal slope parameter that one would observe at infinite energy if the quark model were exact. Equation (3.19) used in conjunction with Eqs. (3.17) and (3.18) gives

$$1-[1-\epsilon_{NN}(1+\gamma^2 R(\infty))]^{1/2} = \tfrac{3}{2}\{1-[1-\epsilon_{\pi N}(1+\gamma^2 R(\infty))]^{1/2}\}, \quad (3.20)$$

$$\epsilon_{KN} = \epsilon_{\pi N}, \quad (3.21)$$

and, inserting numerical values,

$$\epsilon_{\pi N}=(4.64b^U-6.86)/(b^U)^2, \tag{3.22}$$

where $b^U$ is in units of $(\mathrm{GeV}/c)^{-2}$. Using the values of $\epsilon_{NN}$, $\epsilon_{\pi N}$, and $\epsilon_{KN}$, calculated in terms of the universal slope parameter, the slopes at infinite energy *extrapolated from experiment*, $b^{NN}(\infty)$, $b^{\pi N}(\infty)$, and $b^{KN}(\infty)$ can be calculated as

$$b^{xy}(\infty)=\frac{\sigma_T{}^{xy}(\infty)[1+R(\infty)]}{8\pi[1-\{1-\epsilon_{xy}[1+R(\infty)]\}^{1/2}]}, \tag{3.23}$$

where $\sigma_T{}^{xy}(\infty)$ are the total cross sections at infinite energy extrapolated from experiment. Notice, for example, that $b^{KN}(\infty)=b^{\pi N}(\infty)[\sigma_T{}^{KN}(\infty)/\sigma_T{}^{\pi N}(\infty)]$ because $\epsilon_{KN}=\epsilon_{\pi N}$. We see that all of the $b$'s at infinite energy and the constant $\epsilon$'s are determined in terms of one scale fixing parameter $b^U$ and the extrapolated total cross sections.

## IV. NUMERICAL RESULTS AND COMPARISON WITH EXPERIMENTS

The total cross sections[14] and the low-energy elastic-scattering cross sections[15] for different processes will be used as input information in addition to the single universal slope parameter, which is chosen for a fit to all processes at high energies. We will approximate the elastic cross sections in Eq. (2.29) for $D(s_1)$ by

$$\sigma_{\mathrm{el}}(s_1)=[\sigma_T(s_1)]^2/16\pi b(s_1), \tag{4.1}$$

which we expect to be valid for values of $s_1$ large enough so that the upper vertex of Fig. 2 is diffractive. That limit for $s_1$ will be described later in this section.

Using Eq. (4.1), our expression for $D^{xp}(s_1)$,

$$D^{xp}(s_1)\simeq\frac{b^{xp}(s)}{\sigma_T{}^{xp}(s)^2}\left[\frac{2\sigma_T{}^{x\pi^+}(s_1)^2}{b^{x\pi^+}(s_1)}+\frac{\sigma_T{}^{x\pi^0}(s_1)^2}{b^{x\pi^0}(s_1)}\right], \tag{4.2}$$

can be treated in an iterative fashion. Evidently, it contains the quantities we wish to calculate, namely, the $b$'s. However, when Eq. (4.2) is substituted into Eq. (2.22) for $R^{xp}(s)$ and that, in turn, is substituted into Eq. (3.14) for $b^{xp}(s)$, one finds that the result is not sensitive to the input $b$'s of Eq. (4.2). Therefore, one can begin by approximating $b^{xp}(s)=b^U(\infty)$ in Eq. (4.2). This lowest-order approximation is satisfactory for calculating $b(s)$ for $\pi^+p$ and $K^\pm p$. That is because the $b$'s have weak energy dependence and nearly the same size. For $\bar{p}p$, the slope is very much larger and more energy-dependent than the others, so that one must iterate for accuracy. For $\pi^-p$ and $pp$ we must iterate, because Eq. (3.14) develops an imaginary square root (for $p_{\mathrm{lab}}\lesssim 7$ GeV/$c$) in lowest-order approximation. This problem is eliminated by iteration or self-consistent solution. In this paper, we will not iterate the $\pi^-p$ solution beyond the lowest order because it will not be as simple as the iteration for $pp$ and $\bar{p}p$. This last fact is because the input $b^{\pi\pi}(s_1)$, which needs to be used in Eq. (4.2) to calculate $D^{\pi^-p}(s_1)$, is energy-dependent. As explained at the end of Sec. V, our model could be used to predict $b^{\pi\pi}(s_1)$ given $\sigma_T{}^{\pi\pi}(s_1)$; however, this cross section is only known at present via the quark model.

The approximation (4.2) differs appreciably from the actual $D^{pp}(s_1)$ for $s_1<4.53$ GeV$^2$, i.e., the laboratory momentum at the upper $\pi p$ vertex is smaller than 2 GeV/$c$. Therefore, in that region, the experimental data for $\pi p$ elastic cross section will be used. The constant $\alpha$, appearing in the correction factor $\phi(\Delta^2)$, is taken to be $90\mu^2$, which is determined by fitting the reaction cross section of one-pion production at low energies.[10] Similarly, the $D(s_1)$ function for $\pi p$ and $Kp$ can be obtained, except that the energy at which the approximation analogous to Eq. (4.2) breaks down will be lower, i.e., the experimental data on $\pi\pi$ and $K\pi$ elastic cross sections will be used when $s_1<(25/36)(4.53)=3.14$ GeV$^2$. The factor 25/36 is introduced to ensure that the quark-quark pair will have the same amount of energy in $\pi p$, $\pi\pi$, and $K\pi$ scattering. That is to say, we will use Eq. (4.2) for $D^{xp}(s_1)$, when the quark-quark pair has energy greater than $\frac{1}{2}\sqrt{3.14}$ GeV. Unfortunately, the available data on $\pi\pi$ and $K\pi$ elastic cross sections do not extend up to $s_1=3.14$ GeV$^2$. A linear extrapolation is used to connect the data points to the region where $s_1\gtrsim 3.14$ GeV$^2$. The data on $K\pi$ scattering are still rather primitive. We assume them to be dominated by a $P$-wave resonance [i.e., $K^*(891)$] in order to obtain $\sigma_{\mathrm{el}}{}^{K^+\pi^-}$ from the experimental cross section of $K^-\pi^0\to\bar{K}^0\pi^-$. The elastic cross section for $K^-\pi^-$ is chosen to be 3 mb up to $s_1=3.14$ (GeV/$c$)$^2$ which is obtained by Wojcicki *et al.*[15] by assuming that all the events with small momentum transfer are produced by the OPE diagram. Furthermore, whenever the elastic-scattering cross section for a neutral particle in the low-energy region is needed but not available from experiment, we assume it to be the average of the elastic-scattering cross sections for its corresponding positive- and negative-charge particles. Other constants used in the calculation are $\sigma_T{}^{NN}(\infty)=39$ mb and $\sigma_T{}^{K^+p}(s)=\sigma_T{}^{KN}(\infty)=17.2$ mb (obtained by averaging over the

[14] Total cross sections for $pp$: K. J. Foley, R. S. Jones, S. J. Lindenbaum, W. A. Love, S. Ozaki, E. D. Platner, C. A. Quarles, and E. H. Willen, Phys. Rev. Letters **19**, 857 (1967); for $\pi^\pm p$: K. J. Foley, R. S. Jones, S. J. Lindenbaum, W. A. Love, S. Ozaki, E. D. Platner, C. A. Quarles, and E. H. Willen, *ibid.* **19**, 330 (1967); for $K^\pm p$ and $\bar{p}p$: W. Galbraith, E. W. Jenkins, T. F. Kycia, B. A. Leontic, R. H. Phillips, A. L. Read, and R. Rubinstein, Phys. Rev. **138**, B913 (1965).

[15] Elastic cross sections for $\pi^\pm p$: G. Bizard, J. Duchon, J. Sequinot, J. Yonnet, P. Bareyre, C. Bricman, G. Vallades, and G. Villet, Nuovo Cimento **44A**, 999 (1966), J. A. Helland, C. D. Wood, T. J. Devlin, D. E. Hagge, M. J. Longo, B. J. Moyer, and V. Perez-Mendez, Phys. Rev. **134**, B1079 (1964); L. W. Jones, W. L. Kwan, M. L. Perl, S. Ting, V. Cook, B. Cork, and W. Holley, in *Proceedings of the International Conference on High-Energy Physics, Geneva, 1962*, edited by J. Prentki (CERN, Geneva, 1962); for $\pi\pi$: G. Wolf, Phys. Letters **19**, 328 (1965); for $K\pi$: S. G. Wojcicki, Phys. Rev. **135**, B484 (1964).

TABLE II. The calculated ratios $R(s)$ for different processes at various energies.

| $s$ (GeV$^2$) | | 10 | 11 | 12 | 16 | 20 | 24 | 28 | 32 | 36 | 40 |
|---|---|---|---|---|---|---|---|---|---|---|---|
| $R(s)$ | $pp$ | 0.687 | 0.671 | 0.660 | 0.602 | 0.559 | 0.515 | 0.497 | 0.475 | 0.461 | 0.448 |
| | $\bar{p}p$ | 0.472 | 0.466 | 0.454 | 0.438 | 0.426 | 0.419 | 0.408 | 0.402 | 0.400 | 0.396 |
| | $\pi^+p$ | 0.753 | 0.708 | 0.667 | 0.548 | 0.476 | 0.430 | 0.400 | 0.378 | 0.362 | 0.351 |
| | $\pi^-p$ | 1.325 | 1.202 | 1.100 | 0.826 | 0.678 | 0.590 | 0.534 | 0.495 | 0.468 | 0.447 |
| | $K^+p$ | 0.659 | 0.617 | 0.577 | 0.464 | 0.404 | 0.370 | 0.350 | 0.338 | 0.330 | 0.324 |
| | $K^-p$ | 0.487 | 0.447 | 0.412 | 0.329 | 0.305 | 0.299 | 0.287 | 0.279 | 0.271 | 0.265 |
| $p_{\text{lab}}(s)$ (GeV/$c$) | $NN$ | 4.29 | 4.83 | 5.38 | 7.53 | 9.67 | 11.81 | 13.95 | 16.09 | 18.22 | 20.36 |
| | $\pi N$ | 4.85 | 5.38 | 5.91 | 8.05 | 10.18 | 12.31 | 14.42 | 16.57 | 18.71 | 20.84 |
| | $KN$ | 4.70 | 5.24 | 5.77 | 7.91 | 10.05 | 12.18 | 14.31 | 16.45 | 18.58 | 20.71 |

TABLE III. Energy dependence of the slopes in the range of total energy squared $s$ from 10 to 40 GeV$^2$.

| Process | $pp$ | $\bar{p}p$ | $\pi^+p$ | $\pi^-p$ | $K^+p$ | $K^-p$ |
|---|---|---|---|---|---|---|
| $\Delta b(s)$ (GeV/$c$)$^{-2}$ | +1.38 | −3.09 | −0.40 | +0.21[a] | +0.52 | −0.84 |
| Gross behavior | Shrinkage | Growth | Constancy | Constancy | Shrinkage | Growth |

[a] The variation in $b^{\pi^-p}$ is in the range of $s$ from 16 to 40 GeV$^2$.

$K^+p$ total cross section in the $p_{\text{lab}}$ range from 6 to 20 GeV/$c$). The $R$'s can now be calculated and are listed in Table II.

The universal slope parameter is chosen to be 8.44 (GeV/$c$)$^{-2}$. Then the observed slopes at infinite energy for $NN$, $\pi N$, and $KN$ elastic scattering have the values

$$b^{NN}(\infty)=10.1\ (\text{GeV}/c)^{-2},\quad b^{\pi N}(\infty)=8.61\ (\text{GeV}/c)^{-2},\quad \text{and}\quad b^{KN}(\infty)=6.4\ (\text{GeV}/c)^{-2}, \tag{4.3}$$

while the opacities $\epsilon_{NN}$, $\epsilon_{\pi N}$, and $\epsilon_{KN}$ are 0.592,[16] 0.446, and 0.446, respectively. The slopes at finite energies are shown in Figs. 3(a)–3(f) along with those obtained by fitting the observed differential elastic-scattering cross sections at small angles.[17,18] The shrinkage or growth of the slopes in the range of $s=10$ (GeV/$c$)$^2$ to $s=40$ GeV$^2$ (i.e., $p_{\text{lab}}$ from $\simeq$4 to $\simeq$20 GeV/$c$) are shown in Table III. In general, the curves agree well with experiments, except for the early termination of the $\pi^-p$ curve, which has been pointed out previously, and for the energy dependence of $K^+p$. For $K^+p$, the energy dependence of the slope is too weak, and is probably due to an underestimation of the quasielastic cross section. We cannot remedy this discrepancy until the low-energy $K\pi$ and $\pi\pi$ elastic scattering are better understood.

The energy spectrum of the $pp$ scattering has been measured by Anderson *et al.*[6] In order to check our $R^{pp}(s)$ qualitatively, we can obtain the ratio of the experimental quasielastic cross section to the elastic cross section, $R_{\text{expt}}{}^{pp}(s)$, by assuming that the quasielastic scattering has the same $t$ dependence as the elastic scattering and has the spectral shape shown in Fig. 4 which, in principle, can be determined by our OPE diagram. However, in this paper, we do not actually calculate the shape but simply choose it as indicated in the graphs of Drell *et al.*[7] and of Islam.[19] The ratios $R_{\text{expt}}{}^{pp}(s)$ are shown in Table IV along with the theoretical calculation, $R^{pp}(s)$. There are some uncertainties which lead to the discrepancy between $R_{\text{expt}}{}^{pp}(s)$ and $R^{pp}(s)$. At $p_{\text{lab}}\lesssim 6$ GeV/$c$, the distinction between the quasielastic scattering and the uncorrelated production will not be so clear as at higher energies. Consequently, the uncorrelated production region may extend significantly into the quasielastic region and leads to an overestimation of $R_{\text{expt}}{}^{pp}(s)$. Second, the shape we chose

[16] The value 0.592 is the result from the lowest-order approximation while the second iteration gives 0.584.

[17] Unlike all the other data, the $\bar{p}p$ slope has been fit to the form $d\sigma/dt=\exp(a+bt)$ rather than $d\sigma/dt=\exp(a+bt+ct^2)$. Different values of $b$ result from these different fits. These $\bar{p}p$ $b$ values have been increased by 1 (GeV/$c$)$^{-2}$ to put them on the same footing with the slopes for other processes.

[18] Slopes for $pp$: M. L. Perl, L. W. Jones, and C. C. Ting, Phys. Rev. **132**, 1252 (1963); D. Harting, P. Blackall, B. Eisner, A. C. Helmholz, W. C. Middelkoop, B. Powell, B. Zacharov, P. Zanella. P. Dalpiaz, M. N. Focacci, S. Focardi, G. Giacomelli, L. Monari, J. A. Beaney, R. A. Donald, P. Mason, L. W. Jones, and D. O. Caldwell, Nuovo Cimento **38**, 60 (1965); K. J. Foley, S. J. Lindenbaum, W. A. Love, S. Ozaki, J. J. Russell, and L. C. L. Yuan, Phys. Rev. Letters **11**, 425 (1963); **15**, 45 (1965); for $\bar{p}p$: O. Czyzewski, B. Escoubes, Y. Goldschmidt-Clermont, M. Guinea-Moorhead, D. R. O. Morrison, and S. De Unamuno-Escoubes, Phys. Letters **15**, 188 (1965); K. J. Foley, S. J. Lindenbaum, W. A. Love, S. Ozaki, J. J. Russell, and L. C. L. Yuan, Phys. Rev. Letters **11**, 503 (1963); for $\pi^\pm p$: M. L. Perl *et al.*, Phys. Rev. **132**, 1252 (1963); K. J. Foley *et al.*, Phys. Rev. Letters **11**, 425 (1963); for $K^+p$: W. De Baere, J. Debaisieux, P. Dufour, F. Grard, J. Heughebaert, L. Pape, P. Peters, F. Vrebeure, R. Windmolders, R. George, Y. Goldschmidt-Clermont, V. P. Henai, B. Jongejans, D. W. G. Leith, A. Moisseev, F. Muller, J. M. Perreau, and V. Yarba, Nuovo Cimento **45**, 885 (1966); J. Debaisieux, F. Grard, J. Heughebaert, L. Pape, R. Windmolders, R. George, Y. Goldschmidt-Clermont, V. P. Henri, D. W. G. Leith, G. R. Lynch, F. Muller, J. M. Perreau, G. Otter, and P. Sallstrom, *ibid.* **43A**, 142 (1966); W. Chinowsky, G. Goldbaher, S. Goldhaber, T. O'Halloran, and B. Schwarzschild, Phys. Rev. **139**, B1411 (1965); K. J. Foley *et al.*, Phys. Rev. Letters **11**, 503 (1963); for $K^-p$: Aachen-Berlin-CERN-London-Vienna Collaboration, Aderholz *et al.*, Phys. Letters **24B**, 434 (1967); K. J. Foley *et al.* Phys. Rev. Letters **11**, 503 (1963); **15**, 45 (1965); M. N. Focacci, S. Focardi, G. Giacomelli, L. Monari, P. Serra, and M. P. Zerbetto, Phys. Letters **19**, 441 (1965); J. Gordon, *ibid.*, **21**, 117 (1966); J. Mott, R. Ammar, R. Davis, W. Kropac, A. Cooper, M. Derrick, T. Fields, L. Hyman, J. Lorken, F. Schweingruber, and J. Simpson, *ibid.* **23**, 171 (1966).

[19] M. M. Islam, Phys. Rev. **131**, 2292 (1963).

to determine $R_{\text{expt}}{}^{pp}(s)$ has an uncertainty. On the other hand, it is always our belief that the correction factor used in the OPE diagram has, at least, a weak energy dependence. Such an energy dependence may have already manifested itself even at lower energy $p_{\text{lab}}\simeq 2$ GeV/$c$, as indicated in the work by Ferrari and Selleri.[10] We notice that $R_{\text{expt}}{}^{pp}(s)$ has a stronger energy dependence than $R^{pp}(s)$. The slope obtained by using $R_{\text{expt}}{}^{pp}(s)$ in Eq. (3.14), therefore, will have a somewhat stronger shrinkage.

## V. REMARKS

In our analysis, we assumed the scattering amplitude to be pure imaginary. As experiment indicates, the differential elastic-scattering cross section for small momentum transfer can be fitted satisfactorily by the form

$$d\sigma/dt=[\sigma_T(s)/16\pi][1+X^2(s)]e^{bt+ct^2}, \qquad (5.1)$$

where $X(s)$ is the ratio of real to imaginary part in the forward direction. This suggests that the real part of the

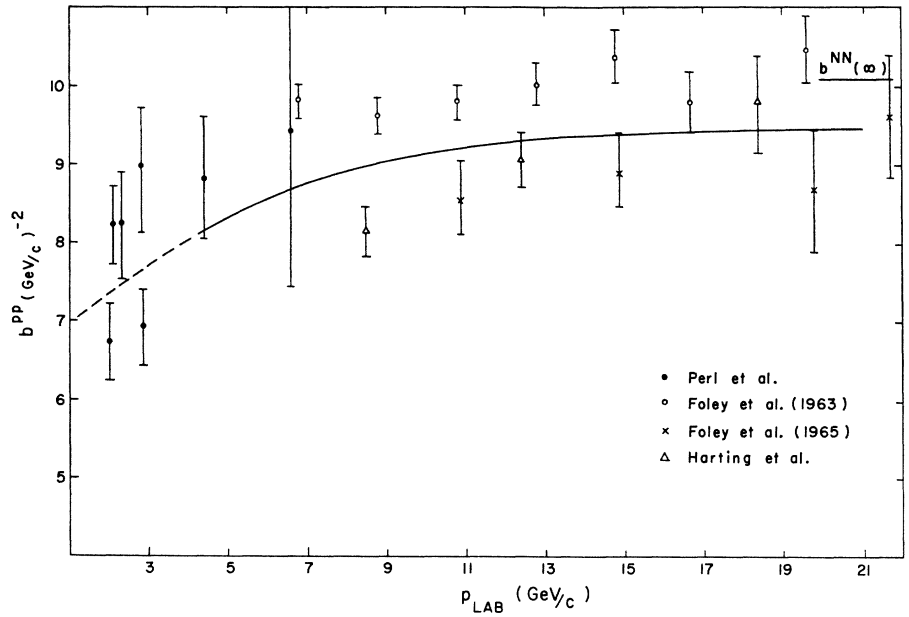


(a)

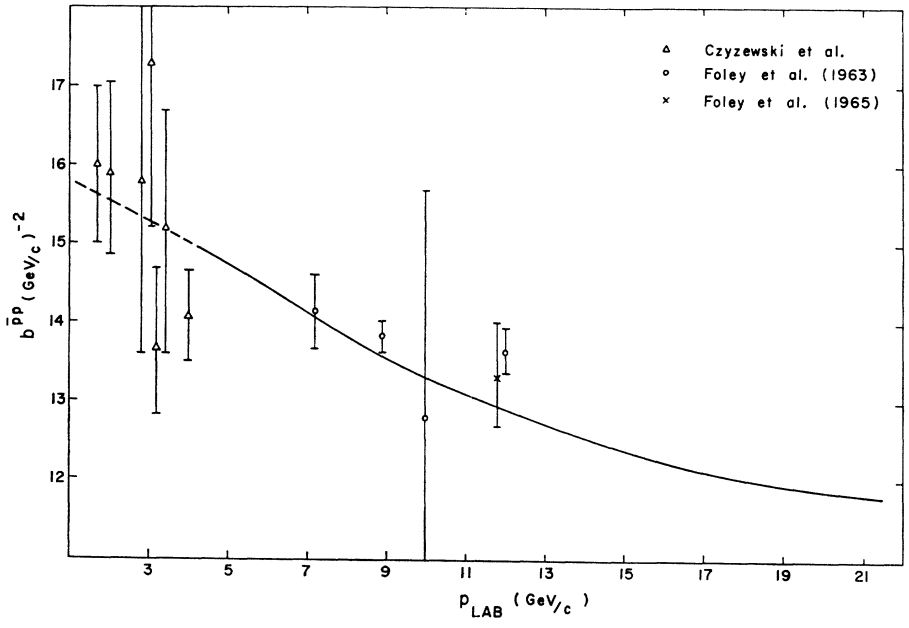


(b)

FIG. 3. The experimental slopes from Ref. 18 for (a) $pp$, (b) $p\bar{p}$, (c) and (d) $\pi^{\pm}p$, and (e) and (f) $K^{\pm}p$ elastic diffraction peaks are compared with our predictions (solid curves) up to $p_{\text{lab}}=21$ GeV/$c$. The extrapolation from our predictions to the intermediate-energy region ($p_{\text{lab}}\lesssim 4$ GeV/$c$) is represented bythe dashed curves.

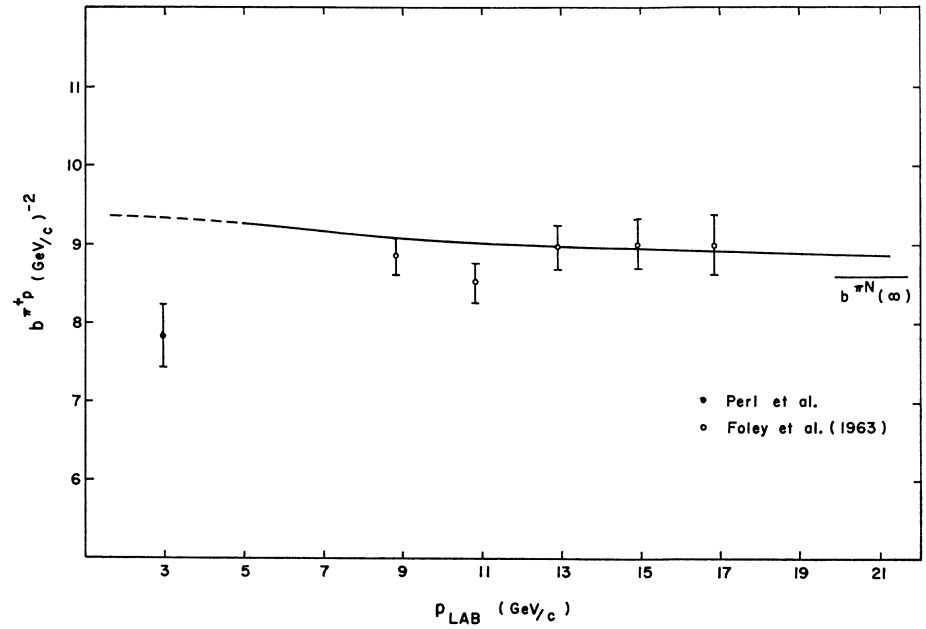


(c)

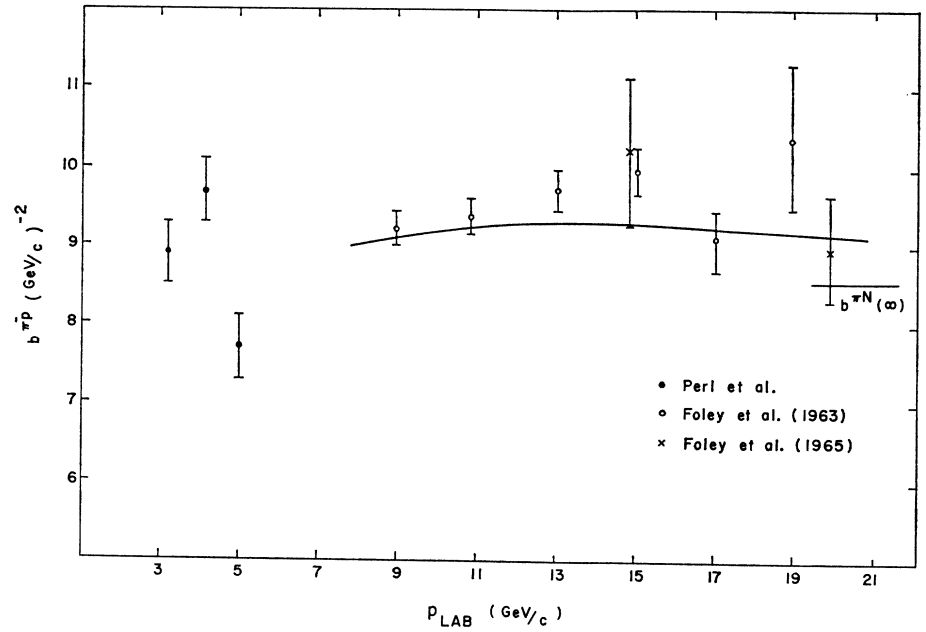


(d)

FIG. 3 (*Continued*)

scattering amplitude has the same small-angle $t$ dependence as the imaginary part. Bellettini *et al.*[20] studied $pp$ scattering at $p_{\text{lab}}=10$, 19, and 26 GeV/$c$ in range of very small angles, extending into the Coulomb-interference region. With the same $t$ dependence for

[20] G. Bellettini, G. Cocconi, A. N. Diddens, E. Lillethum, J. Pahl, J. P. Scanlon, J. Walters, A. M. Wetherhell, and P. Zanella, Phys. Letters **14**, 164 (1965).

TABLE IV. Ratios of $pp$ obtained by direct calculation $[R^{pp}(s)]$ and by fitting the energy spectrum $[R_{\text{expt}}{}^{pp}(s)]$.

| $p_{\text{lab}}$ (GeV/$c$) | 6.1 | 9.9 | 15.1 | 20 | $\infty$ |
|---|---|---|---|---|---|
| $R^{pp}(s)$ | 0.64 | 0.555 | 0.485 | 0.45 | 0.327 |
| $R_{\text{expt}}{}^{pp}(s)$ | 0.734 | 0.475 | 0.3355 | 0.29 | 0.25 |

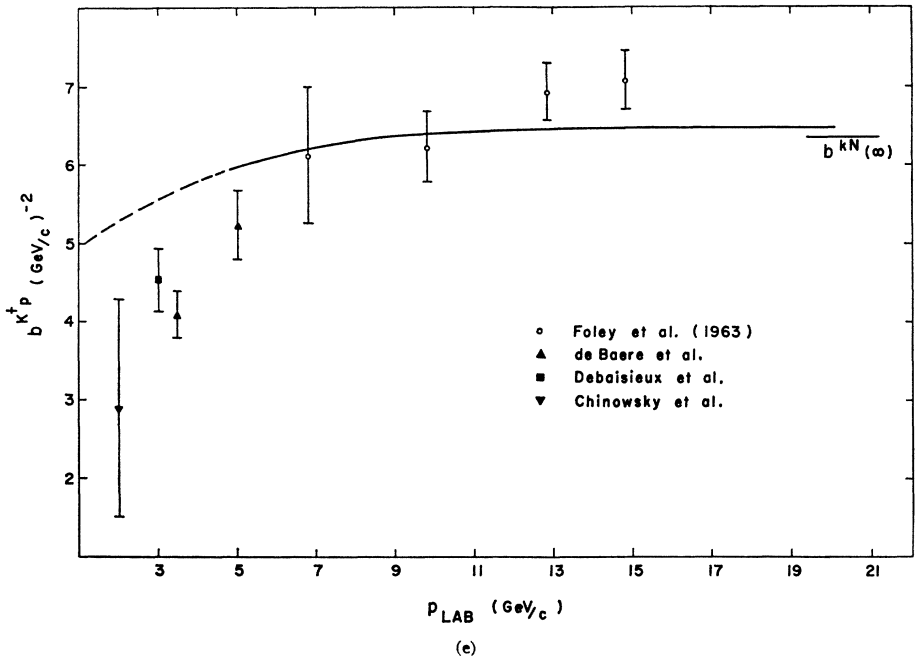


(e)

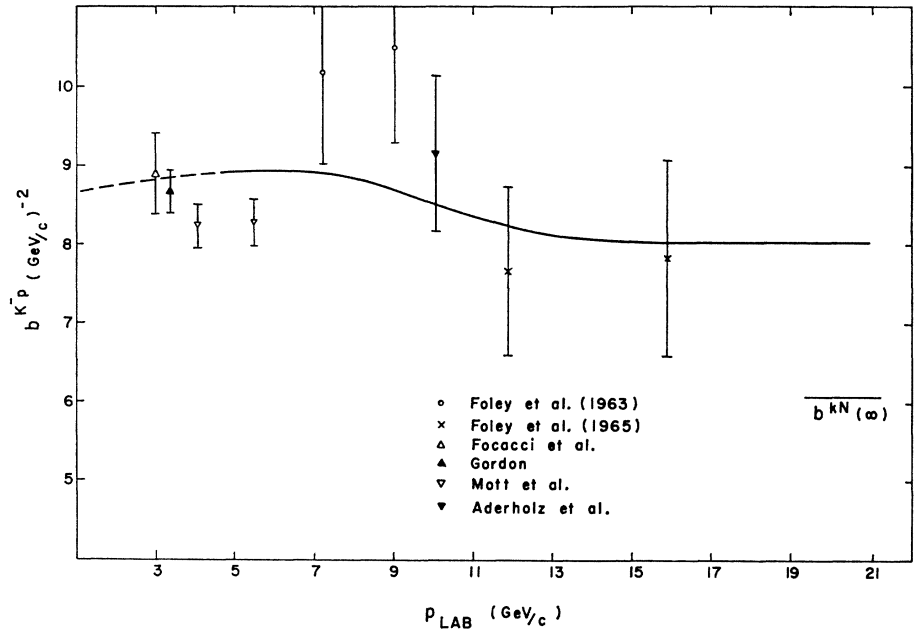


(f)

FIG. 3 (*Continued*)

both real and imaginary parts, a very good fit to the data was obtained. If we assume this fact to be also true for small angles, our formula for the slope becomes

$$b(s)=\frac{\sigma_T(s)[1+R(s)][1+X^2(s)]}{8\pi[1-\{1-\epsilon[1+R(s)][1+X^2(s)]\}^{1/2}]}. \quad (5.2)$$

Experimentally, only $X^{pp}(s)$ is not negligible. If we take $X^{pp}(s)$ into account, a slightly better fit to $b^{pp}(s)$ will result.

If we do not approximate the relation $g_Q{}^{\pi N}(s,t) \propto g_{el}{}^{\pi\pi}(st)$ by $g_Q{}^{\pi N}(s,t) \propto g_{el}{}^{\pi N}(s,t)$ [cf. Eqs. (2.16)–(2.19)], we can proceed in the following way: Choosing $\epsilon_{\pi\pi}$ as a parameter, $b^{\pi\pi}(s)$ can be determined by the $\pi\pi$ total cross sections which can be obtained by means of

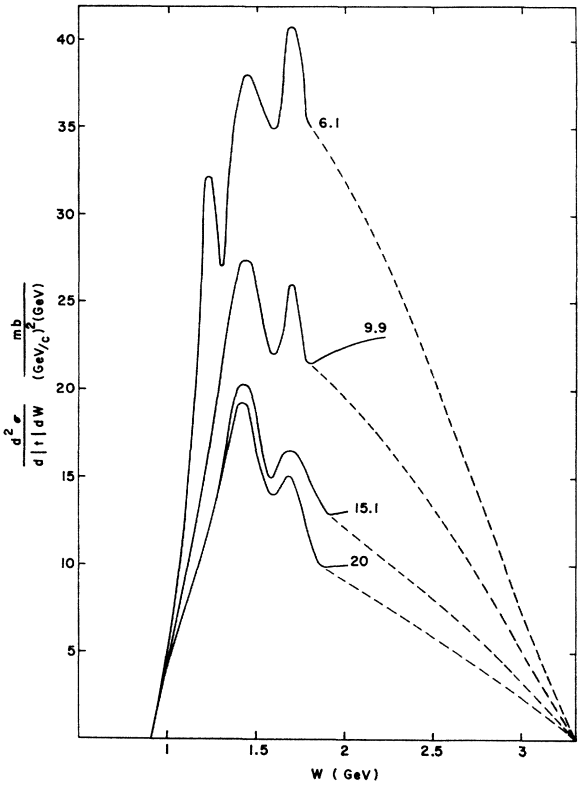


FIG. 4. The spectral shapes used to evaluate $R_{\text{expt}}{}^{pp}(s)$ are represented by the dashed curves. The doubly differential cross sections from Ref. 6, $d^2\sigma/d|t|dW$, as $p_{\text{lab}}$ varying from 6.1 to 20 GeV/$c$ and $|t|$ fixed at 0.042 (GeV/$c$)$^2$ are denoted by the solid curves. The invariant missing mass is $W$.

the quark model. With known $b^{\pi\pi}(s)$, we can determine $b^{\pi N}(s)$ through Eq. (3.10) and the $\pi N$ unitarity condition, that

$$\text{Im}h_l{}^{\pi N}(s)=|h_l{}^{\pi N}(s)|^2+|h_l{}^{\pi\pi}(s)|^2\Gamma^{\pi N}(s,0)+\tfrac{1}{4}\rho_l(s)^{\pi N}, \quad (5.3)$$

and then determine $b^{NN}(s)$ through Eq. (3.10) and the $NN$ unitarity condition

$$\text{Im}h_l{}^{NN}(s)=|h_l{}^{NN}(s)|^2+|h_l{}^{\pi N}(s)|^2\Gamma^{NN}(s,0)+\tfrac{1}{4}\rho_l(s)^{NN}. \quad (5.4)$$

Because the $pp$ total cross section stays almost constant, it can be shown that the $pp$ peak shrinks even if $b^{\pi N}(s)$ is a constant and different from $b^{NN}(s)$. Thus, approximation (2.19) can be relaxed without significantly affecting the results.

In our calculation, we have used a grey-sphere shape for $\rho_l$. It is important to inquire whether the slopes are significantly affected by choosing other shapes for the Van Hove overlap function. One basic fact about $\rho_l(s)$ to bear in mind is that this function cannot be wholly arbitrary but must satisfy several constraints: first, a modified unitarity constraint from Eq. (3.11) that $\rho_l(s)<[1+R(s)]^{-1}$ for any $l$ or any $s$ in the range of interest; second, that $\rho_l(s)$ has $l$ dependence such that the slopes at infinite energy have the desired values. For example, a two-parameter Gaussian shape will not satisfy these first two constraints simultaneously. Next we require that the average opacity as defined in Eq. (3.12) be independent of energy for $p_{\text{lab}}\geqslant 4$ GeV/$c$. Finally, we require that $\rho_l(s)$ be chosen so that Eqs. (3.7) and (3.11) give the *observed* total cross section. These constraints are quite restrictive. For example, they guarantee that the difference between slopes calculated by two different two-parameter shapes of $\rho_l(s)$ will be proportional to $dR(s)/ds$ and also to the difference of the $\rho$'s averaged by an integration. In the case of $\bar{p}p$ scattering, where $dR(s)/ds$ is very small, any acceptable shape will give the same slope as a function of $s$.

Let us consider the special case of two-parameter shapes for $\rho_l$ in greater detail. We will work, for convenience, in the impact parameter representation[3] where partial-wave sums are replaced by integrals. The most general two-parameter shape is

$$\rho^{\text{V.H.}}(d,s)=\xi f(d/R_{\text{V.H.}}(s)), \quad (5.5)$$

where $d$ is the impact parameter. This form has the property that $\epsilon(s)$ from Eq. (3.12) is a constant if the parameter $\xi$ of Eq. (5.5) is constant. The total cross section is determined by $R_{\text{V.H.}}(s)$, which fixes that energy-dependent parameter. Then the slope is just

$$b(s)=\frac{\sigma_T(s)[1+R(s)]}{8\pi}\times\int_0^\infty dx\, x^3\{1-[1-\xi f(x)(1+R(s))]^{1/2}\}\times\left(\int_0^\infty dx\, x\{1-[1-\xi f(x)(1+R(s))]^{1/2}\}\right)^{-2}, \quad (5.6)$$

where the variable $x$ is equal to $d/R_{\text{V.H.}}(s)$. The final parameter $\xi$ is fixed by using Eq. (5.6) as $s\to\infty$ and the scale-fixing value $b(\infty)$ as determined by Eq. (4.3). Now let us investigate a shape which is quite different from the grey sphere but for which the integrals involved in calculating the total cross section and the slope can be carried out explicitly. A shape linear in $x^2$ is chosen,

$$\rho^{\text{V.H.}}(d,s)=\xi\{1-[d/R_{\text{V.H.}}(s)]^2\}\theta(R_{\text{V.H.}}(s)-d). \quad (5.7)$$

Consider $\pi^+p$ scattering in particular. The parameters $\xi$ and $R_{\text{V.H.}}{}^2(\infty)$ are found to be 0.579 and 54.3 (GeV/$c$)$^{-2}$, respectively. The respective grey sphere and linear shapes, fixed to satisfy the preceding constraints, are shown in Fig. 5. The slopes are shown in Fig. 6. The maximum difference between slopes calculated by the linear shape and the grey-sphere shape in the range of $p_{\text{lab}}$ shown in Fig. 6 is approximately 5%. We believe that the actual shape of $\rho_l{}^{\text{V.H.}}(s)$ cannot differ from the grey-sphere shape by as much as the linear shape.

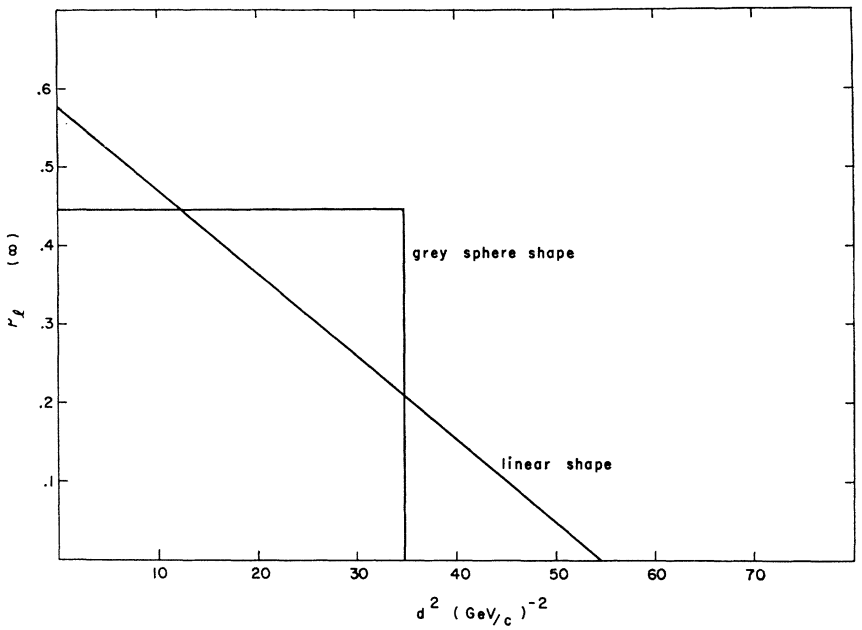


FIG. 5. Grey-sphere shape and linear shape for $\rho_l^{\text{V.H.}}(s)^{\pi^+p}$.

Therefore, we believe that the slopes are not significantly affected by choosing different shapes for $\rho_l^{\text{V.H.}}(s)$ which satisfy the preceding constraints.

We expect that our model, without modifications, will break down at $p_{\text{lab}} \lesssim 2$ GeV/$c$. Among various reasons, the most important ones are the following: First, the real part of the scattering amplitude becomes important, and the elastic scattering is not just simply the shadow of the inelastic channels. Second, the average transparency cannot be a constant in the low-energy region since it must drop to zero at the inelastic threshold.

In conclusion, we believe that the energy dependence of the widths of the diffraction peaks for hadron elastic scattering at small $t$ is an interplay between the energy dependence of the total cross section and the quasi-elastic cross section, while the magnitude of the widths is a manifestation of the size of the interaction radius. At high energies, the diffraction elastic scattering does not require complicated dynamics for explanation. Similarly, we believe that the total cross section also does not depend on detailed dynamics. It may only depend on general properties of the interaction, e.g.,

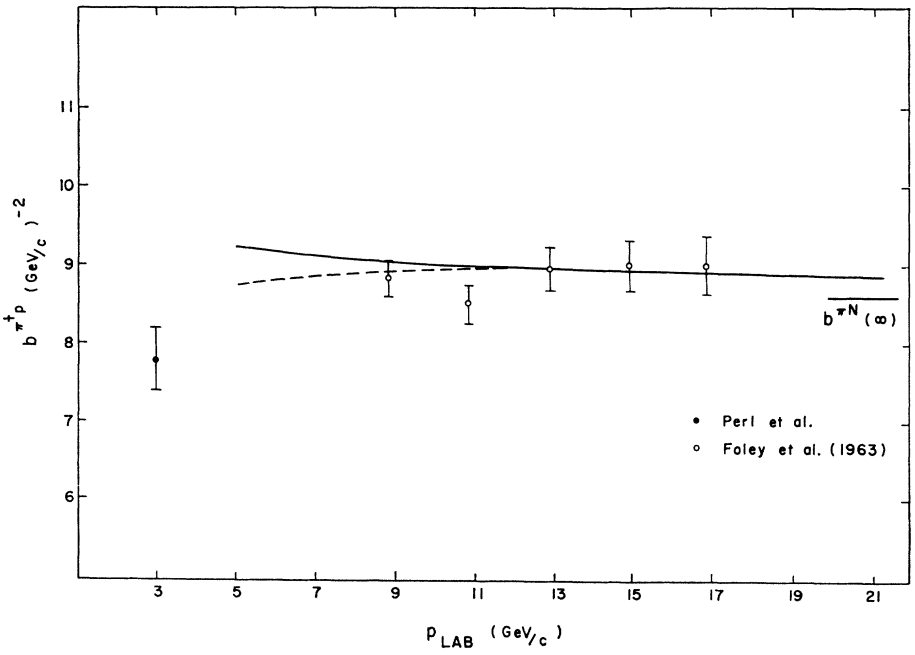


FIG. 6. $\pi^+p$ slopes for $\rho_l^{\text{V.H.}}(s)$ to be linear (dashed curve) and a grey sphere (solid curve).

coupling constant, number of inelastic channels, phase space, statistical counting, etc. Dynamics may then be needed only for explaining a particular channel whose contribution tends to vanish as energy increases. Therefore, it would appear that the low-energy resonance region has greater dynamical content than the high-energy domain studied in this paper. Our model also suggests that the analysis of inelastic collisions will be simplified if the quasielastic part is removed. Concerning experiments in the future, it is desirable to measure the energy spectra for $\pi^{\pm}p$, $K^{\pm}p$, and $\bar{p}p$ scattering so that our calculated $R(s)$ can be checked, at least qualitatively, by experiments. Finally, we notice an interesting prediction on the width of $\pi\pi$ elastic diffraction scattering. According to our model, the quasielastic scattering for all processes is mainly due to the OPE diagram. However, such a diagram is forbidden in $\pi\pi$ scattering by G parity. We expect that the contribution due to other diagrams is very small. As a consequence, the quasielastic cross section for $\pi\pi$ will be very small. If the $\pi\pi$ total cross section behaves like all other total cross sections (i.e., does not increase with increasing energy), we predict that *shrinkage of the $\pi\pi$ diffraction peak is impossible.*

## ACKNOWLEDGMENTS

The authors would like to acknowledge enlightening discussions held with Professor L. L. Foldy, Professor L. Kisslinger, Professor R. M. Thaler, Professor P. B. Kantor, and many other members of the Case Western Reserve University high-energy group.

PHYSICAL REVIEW VOLUME 184, NUMBER 5 25 AUGUST 1969

# Gauge Theory of Strong Interactions*

P. J. O'Donnell
*Department of Physics, University of Toronto, Canada*
(Received 18 February 1969)

A generalization of gauge invariance in strong interactions is given. This leads naturally to a structure of $[U(3)]^4$ with the gauge fields corresponding to the quantum numbers $J^{PC}=1^{++}$, $1^{+-}$, $1^{--}$, $1^{-+}$. Currents of both first- and second-class types are present. A tentative assignment of the gauge fields to possible resonances is made.

## 1. INTRODUCTION

An important method in considering the symmetries of strong interactions has been to use gauge invariance of a Lagrangian to infer the existence of conserved currents. The gauge invariance is then broken by mass terms for example, resulting in partial-conservation laws. When these conserved or partially conserved currents are assumed to be the currents which describe the electromagnetic and weak interactions, several deep results follow.[1] The spin-1 gauge fields that are inferred by a local gauge invariance of a Lagrangian have been considered to be important because they must belong to the regular representation of the symmetry group. With the recent work of Kroll, Lee, and Zumino[2] and of others,[3] they too have been shown to be important in a dynamical sense in describing the electromagnetic and weak interactions of the hadrons. Since broken $SU(3)$ is well established as an algebraic symmetry, it would seem important to investigate the full consequences of an approach based on successive approximations to a completely exact local gauge invariance. Not only is such a method an important and fundamental way of arriving at the interaction of fields, but it has, in the past, also been used to infer the existence of pionic resonances which are identified with the gauge fields.[4]

In this paper, we examine a generalized application of gauge invariance,[5-7] and arrive at an underlying group structure of $[U(3)]^4$. A tentative assignment of the gauge fields to possible resonances is made.

* Supported in part by the National Research Council of Canada.

[1] S. Adler and R. Dashen, *Current Algebras* (W. A. Benjamin, Inc., New York, 1968).

[2] N. M. Kroll, T. D. Lee, and B. Zumino, Phys. Rev. **157**, 1376 (1967).

[3] T. D. Lee and B. Zumino, Phys. Rev. **163**, 1667 (1967); T. D .Lee, S. Weinberg, and B. Zumino, Phys. Rev. Letters **18**, 1029 (1967).

[4] J. J. Sakurai, Ann. Phys. (N.Y.) **11**, 1 (1960).

[5] The group $[U(3)]^4$ obtained here is not the same as the group obtained previously by the authors listed in Refs. 6 and 7. The transformations which these authors considered may still be applied along with the generalization given here and would result in a doubling of the number of gauge fields.

[6] P. G. O. Freund and Y. Nambu, Phys. Rev. Letters **12**, 714 (1964).

[7] A. Salam and J. C. Ward, Phys. Rev. **136**, B763 (1964). We shall follow the notation of these authors.